

Inelastic nuclear screening for different secondaries produced in p +Pb collisions at LHC energy

G.H. Arakelyan¹, C. Merino², Yu.M. Shabelski³ and A.G. Shuvaev³

¹A.Alikhanyan National Scientific Laboratory (Yerevan Physics Institute)
Yerevan, 0036, Armenia
E-mail: argev@mail.yerphi.am

¹Departamento de Física de Partículas, Facultade de Física
and Instituto Galego de Física de Altas Enerxías (IGFAE)
Universidade de Santiago de Compostela, Galiza, Spain
E-mail: merino@fpaxp1.usc.es

³ Petersburg Nuclear Physics Institute
NCR Kurchatov Institute
Gatchina, St.Petersburg 188300 Russia
E-mail: shabelsk@thd.pnpi.spb.ru
E-mail: shuvaev@thd.pnpi.spb.ru

Abstract

We calculate the inclusive spectra of secondaries produced in soft (minimum bias) p +Pb collisions in the framework of Quark-Gluon String Model at LHC energy, by taking into account the inelastic screening corrections (percolation effects). The role of these effects is expected to be very large at the very high energies, and they should decrease the spectra more than 2 times in the midrapidity region at $\sqrt{s_{NN}} = 5$ TeV. The experimental data confirm such a picture, which means that the nuclear screening effects are connected with the Pomeron interaction rather than with the interactions of the produced secondary particles in the final state.

PACS. 25.75.Dw Particle and resonance production

1 Introduction

The investigation of soft p +Pb interactions is very interesting because it can give the answer to the problem of inelastic shadow corrections [1, 2] for inclusive particle production.

In [1, 2] it was shown that the correct description of the inclusive spectra of secondaries produced in d+Au collisions at $\sqrt{s} = 200$ GeV (RHIC) requires to account for the inelastic shadow corrections, that are probably connected with the multipomeron interactions and that lead to the saturation of the inclusive density of secondary hadrons in the soft (low p_T) region, where the methods based on perturbative QCD cannot be used. The effects of the inelastic shadow corrections should increase with the initial energy. The difference in the results for the spectra obtained from the calculations with and without the inelastic shadow effects at LHC energies is of about a factor 2 in the midrapidity region.

The data for the inclusive densities of all charged secondaries obtained by the ALICE [3] collaboration experimentally confirm the existence of these corrections [5] at the LHC energy $\sqrt{s_{NN}} = 5$ TeV. In principal, two possibilities exist to explain the origin of the inelastic nuclear screening: either it comes from the diagrams with Pomeron interactions, or from the interactions of the produced secondaries with another hadrons and/or Pb nucleus. In the first case, the inelastic screening effects should be the same for different secondaries, while for the second one these effects should depend on the interaction cross sections of the secondaries, so the effects should be different for the different secondaries.

In this paper we compare the experimental data for the inclusive densities of different secondaries obtained by the CMS [4] collaboration to the corresponding predictions of the Quark-Gluon String Model (QGSM) [6, 7] for p +Pb at $\sqrt{s_{NN}} = 5$ TeV.

The QGSM quantitatively describes many features of the high energy production processes, including the inclusive spectra of different secondary hadrons produced in the high energy hadron-nucleon [8, 9, 10, 12] and hadron-nucleus collisions [13, 14]. In the frame of the QGSM, the hadron-nucleon interactions have already been considered at different energies, including LHC, whereas the hadron nucleus collisions have been described at not very high energies, where the inelastic screening corrections are negligibly small [1].

Now, at the LHC energies the inelastic screening corrections become large, what allows us to analyze them in more detail.

2 Inclusive spectra of secondary hadrons in the Quark-Gluon String Model

In order to produce quantitative predictions for the inclusive spectra of secondary hadrons, a model for multiparticle production is needed. It is for that purpose that we have used the QGSM [6, 7] in the numerical calculations presented below.

In the QGSM, both high energy hadron-nucleon and hadron-nucleus interactions are treated as proceeding via the exchange of one or several Pomerons, and all elastic and inelastic processes result from cutting through or between Pomerons [15]. Each Pomeron corresponds to a cylinder diagram (see Fig. 1a) that, when cut, produces two showers of secondaries, as it is shown in Fig. 1b. The inclusive spectrum of secondaries is then determined by the convolution of diquark, valence quark, and sea quark distributions in the incident particles, $u(x, n)$, with the fragmentation functions of quarks and diquarks into the secondary hadrons, $G(z)$. Both functions $u(x, n)$ and $G(z)$ are determined by the appropriate Reggeon diagrams [16].

The diquark and quark distribution functions depend on the number n of cut Pomerons in the considered diagram. In the following calculations we use the recipe of reference [13].

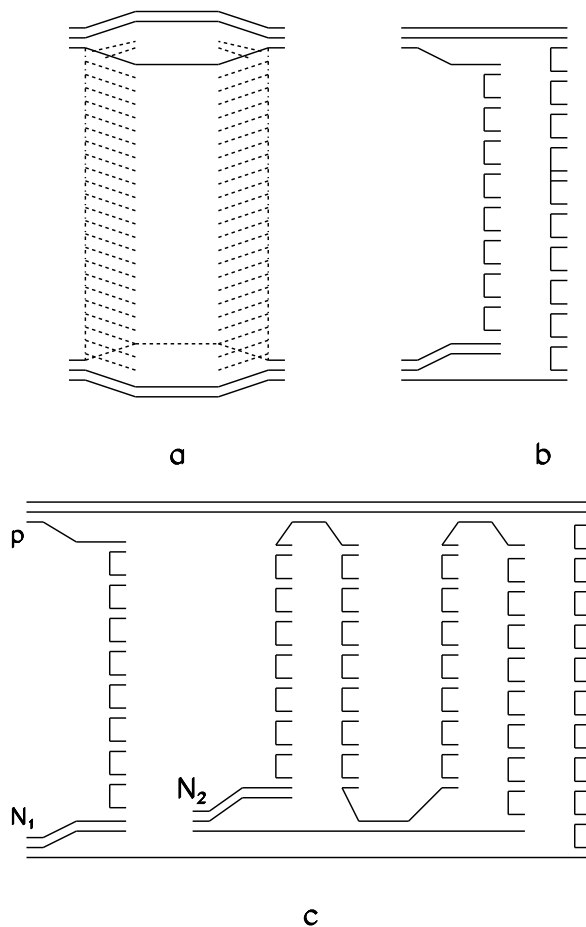


Figure 1: (a) Cylindrical diagram representing the Pomeron exchange within the Dual Topological Unitarization (DTU) classification (quarks are shown by solid lines); (b) Cut of the cylindrical diagram corresponding to the single-Pomeron exchange contribution in inelastic pp scattering; (c) Diagram corresponding to the inelastic interaction of an incident proton with two target nucleons N_1 and N_2 in a pA collision.

For the nucleon target, the inclusive density dn/dy of a secondary hadron h has the

form [6]:

$$\frac{dn}{dy} = \frac{1}{\sigma_{inel}} \cdot \frac{d\sigma}{dy} = \frac{x_E}{\sigma_{inel}} \cdot \frac{d\sigma}{dx_F} = \sum_{n=1}^{\infty} w_n \cdot \phi_n^h(x) \quad , \quad (1)$$

where the functions $\phi_n^h(x)$ determine the contribution of diagrams with n cut Pomerons, and w_n is the probability for this process to occur [17]. Here we neglect the diffractive dissociation contributions that would only be significant in the fragmentation regions, i.e at large x_F .

For pp collisions

$$\phi_n^h(x) = f_{qq}^h(x_+, n) \cdot f_q^h(x_-, n) + f_q^h(x_+, n) \cdot f_{qq}^h(x_-, n) + 2(n-1)f_s^h(x_+, n) \cdot f_s^h(x_-, n) \quad , \quad (2)$$

$$x_{\pm} = \frac{1}{2}[\sqrt{4m_T^2/s + x^2} \pm x] \quad , \quad (3)$$

where f_{qq} , f_q , and f_s are the contributions of diquarks, valence quarks, and sea quarks, respectively.

These contributions are determined by the convolution of the diquark and quark distributions with the fragmentation functions, e.g.,

$$f_q^h(x_+, n) = \int_{x_+}^1 u_q(x_1, n) \cdot G_q^h(x_+/x_1) dx_1 \quad . \quad (4)$$

The diquark and quark distributions, as well as the fragmentation functions, are determined by Regge asymptotics [16]. The numerical values of the model parameters were published in reference [9].

The probabilities w_n in Eq. (1) are the ratios of the cross sections corresponding to n cut Pomerons, $\sigma^{(n)}$, to the total non-diffractive inelastic pp cross section, σ_{nd} [17].

The contribution of multipomeron exchanges in high energy pp interactions results in a broad distribution of w_n (see [5]). In the case of interaction with a nuclear target, the Multiple Scattering Theory (Gribov-Glauber Theory) is used, which allows to treat the interaction with the nuclear target as the superposition of interactions with different numbers of target nucleons. Let $W_{pA}(\nu)$ be the probability for the inelastic interactions of the proton with ν nucleons of the target, and σ_{prod}^{pA} the total cross section of secondary production in a p+A collision. From the Multiple Scattering Theory, one has:

$$W_{pA}(\nu) = \sigma^{(\nu)} / \sigma_{prod}^{pA} \quad , \quad (5)$$

(see again reference [5] for the numerical examples). Here,

$$\sigma^{(\nu)} = \frac{1}{\nu!} \int d^2b \cdot [\sigma_{inel}^{pN} \cdot T(b)]^{\nu} \cdot e^{-\sigma_{inel}^{pN} \cdot T(b)} \quad (6)$$

coincides [18, 19, 20, 21] with the optical model expression [22], and

$$\sigma_{prod}^{pA} = \int d^2b \cdot (1 - e^{-\sigma_{inel}^{pN} \cdot T(b)}) \quad , \quad (7)$$

where $T(b)$ is the profile function of the nuclear target:

$$T(b) = A \int_{-\infty}^{\infty} dz \cdot \rho(b, z) , \quad (8)$$

with $\rho(r = \sqrt{b^2 + z^2})$ the one-particle nuclear density.

The average value of ν has the well-known form:

$$\langle \nu \rangle = \frac{A \cdot \sigma_{inel}^{pp}}{\sigma_{prod}^{pA}} . \quad (9)$$

We use the numerical values $\sigma_{inel}^{pp} = 72$ mb and $\sigma_{prod}^{pPb} = 1900$ mb at $\sqrt{s} = 5$ TeV, so that

$$\langle \nu \rangle_{p+Pb} = 7.8. \quad (10)$$

In the calculation of the inclusive spectra of secondaries produced in pA collisions we should consider the possibility of one or several Pomeron cuts in each of the ν blobs of the proton-nucleon inelastic interactions. For example, in Fig. 1c it is shown one of the diagrams contributing to the inelastic interaction of a beam proton with two nucleons from the target. In the blob of the proton-nucleon(1) interaction one Pomeron is cut, and in the blob of the proton-nucleon(2) interaction two Pomerons are cut. It is essential to take into account all the diagrams with every possible Pomeron configuration and its permutations. The diquark and quark distributions and the fragmentation functions here are the same as in the case of the interaction with one nucleon.

The process shown in Fig. 1c satisfies [18, 19, 20, 21] the condition that the absorptive parts of the hadron-nucleus amplitude are determined by the combination of the absorptive parts of the hadron-nucleon amplitudes.

3 Inclusive spectra in p+A collisions at very high energy and inelastic screening (percolation) effects

The QGSM gives a reasonable description [13, 23] of the inclusive spectra of different secondaries produced in hadron-nucleus collisions at energies $\sqrt{s_{NN}} = 14-30$ GeV.

The situation drastically changes at RHIC energies. The spectra of secondaries produced in pp collisions can be rather well described, but the RHIC experimental data for Au+Au collisions [24, 25] give clear evidence for the inclusive density saturation effects, which reduce the inclusive density about two times in the central (midrapidity) region when compared to the predictions based on the superposition picture [26, 27, 28]. This reduction can be explained by the inelastic screening corrections connected to multi-pomeron interactions [1]. The effect is very small for integrated cross sections (many of them are determined only by geometry), but it is very important [1] for the calculations of secondary multiplicities and inclusive densities at the high energies.

However, all estimations are model dependent. The numerical weight of the contribution of the multipomeron diagrams is rather unclear due to the many unknown vertices. The number of unknown parameters can be reduced in some models, and, for example, in reference [1] the Schwimmer model [29] was used for the numerical estimations.

Another approaches were used in reference[30], where the phenomenological multipomeron vertices of eikonal type were introduced for enhancement diagram summation.

The calculations of inclusive densities and multiplicities, both in pp [31, 32], and in heavy ion collisions [32, 33] (with accounting for inelastic nuclear screening), can be fulfilled in the percolation theory, and they result in a good agreement with the experimental data in a wide energy region.

The percolation model also provides a reasonable description of the transverse momentum distribution (at low and intermediate p_T) including the Cronin effect and the behavior of the baryon/meson ratio [34, 35, 36]. The percolation approach assumes two or several Pomerons to overlap in the transverse space and to fuse in a single Pomeron. When all quark-gluon strings (cut Pomerons) are overlapping, the inclusive density saturates, reaching its maximal value at a given impact parameter.

In order to account for the percolation effects in the QGSM, it is technically more simple [2] to consider in the central region the maximal number of Pomerons n_{max} emitted by one nucleon. After they are cut, these Pomerons lead to the different final states. Then the contributions of all the diagrams with $n \leq n_{max}$ are accounted for as at the lower energies. The unitarity constraint also obeys the emission of the larger number of Pomerons $n > n_{max}$ but due to fusion in the final state (on the quark-gluon string stage) the cut of $n > n_{max}$ Pomerons results in the same final state as the cut of n_{max} Pomerons.

By doing this, all model calculations become rather simple and very similar to those in the percolation approach. The QGSM fragmentation formalism allows one to calculate the spectra of different secondaries integrated over p_T as functions of initial energies, rapidity, and x_F . In this scenario we obtain a reasonable agreement with the experimental data on the inclusive spectra of secondaries at RHIC energy (see [2] with $n_{max} = 13$).

It has been shown in [37] that the number of strings for the secondary production should increase with the initial energy even when the percolation effects are included. Thus, in the following calculations we use the value $n_{max} = 21$ at the LHC energy $\sqrt{s} = 5 \text{ TeV}$, that can be regarded as the normalization of all the charged secondaries multiplicities in the midrapidity region to the ALICE data [3]. The predictive power of our calculation applies for different sorts of secondaries in midrapidity region. If the inelastic nuclear screening comes mainly from the Pomeron interactions, as it was discussed above, the screening effects would be the same for all the secondaries. On the other hand, if the final state absorption of the produced particles are important, nuclear screening effects would be different for different secondaries, i.e. for kaons and antibaryons.

In the following calculations, one additional effect is also taken into account, namely the transfer of the baryon charge to large distances in rapidity space through the string

junction effect [10, 11]. This transfer leads to an asymmetry in the production of baryons and antibaryons in the central region that is non-zero even at LHC energies. In the calculation of these effects, the following values have been chosen for the model parameters [11]:

$$\alpha_{SJ} = 0.5 \text{ and } \varepsilon = 0.0757. \quad (11)$$

4 Rapidity spectra of different secondaries at LHC energies

To compare the calculated effect of nuclear screening with the experimental data, the adequate description of the secondary production on nucleon, as well as on nuclear targets is needed. First, we present the QGSM description of π^\pm , K^\pm , p , and \bar{p} productions in pp collisions at LHC energies, and then we compare the results of our calculations with the experimental data by the CMS Collaboration [4, 38] and by the ALICE Collaboration [39, 40, 41], as it is shown in Fig 2, where, following the analysis published by the ALICE Collaboration [41], the productions of average π , K , and $p\bar{p}$ are presented.

As it can be seen in Fig. 2, the experimental data by the ALICE Collaboration are approximately 20–30% lower than those published by the CMS Collaboration. The agreement of QGSM calculations with both sets of experimental data looks rather reasonable, given that the accuracy of our calculations is estimated to be on the level of a 10–15% theoretical uncertainty.

Now, let us consider the normalization of the QGSM calculations for the case of nuclear targets to the experimental point by the ALICE Collaboration [3], $dn_{ch}/d\eta = 16.81 \pm 0.71$ at $\sqrt{s_{NN}} = 5$ TeV. The agreement is reached at $n_{max} = 21$, here we have $dn/d\eta$ for $|\eta| < 2$. Later, the experimental value $dn/dy(|y| \leq 1) = 19.1 \pm 0.2$ has been published by the CMS Collaboration [4], while the QGSM calculation gives $dn/dy(|y| \leq 1) = 19.11$ with $n_{max} = 21$, so we can use this n_{max} value in our analysis.

The experimental data for p +Pb collisions by the CMS Collaboration on the inclusive densities of different secondaries, π^\pm , K^\pm , p , and \bar{p} [4] are presented in Table 1, where they are compared with our QGSM predictions. The agreement for every secondary particles is good, what it means that the experimental nuclear shadowing factor is the same for different secondaries, as it is assumed in our calculations.

Also in Table 1, we present the QGSM predictions for the pp collisions at the same energy. The ratios of particle yields in p +Pb and pp collisions are equal to 3.6–3.7, i.e they are two times smaller than the values of ν_{p+Pb} in Eq. 10. In the absence of inelastic nuclear screening, the ratio $r = pPb/pp$ in the midrapidity region should be equal to ν_{p+Pb} [18, 19, 20, 21], that is, to the average number of the inelastic collisions of the incident proton in the target nucleus. Thus, we can see that the inelastic nuclear screening factor is little larger than 2, and it is practically the same for all considered secondaries.

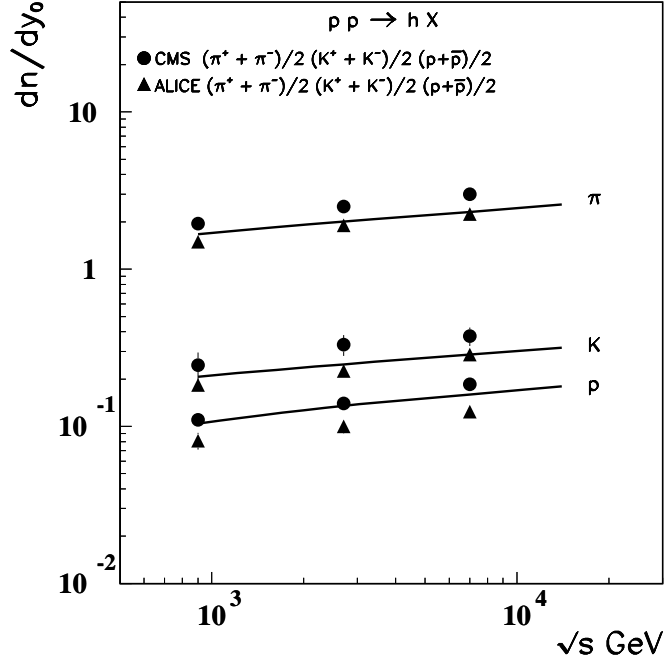


Figure 2: The energy dependence of the rapidity density dn/dy at $y = 0$ of average pions, kaons and protons/antiprotons production in pp collisions. The experimental data are by the CMS Collaboration [38, 4] and by the ALICE collaboration [39, 40, 41]. The theoretical curves represent the result of the corresponding QGSM calculations.

particles	CMS Collaboration $dn/dy, y \leq 1$ [4]	QGSM		
		$p+Pb$	pp	r
π^+	8.074 ± 0.087	8.103	2.190	3.70
π^-	7.971 ± 0.079	7.923	2.147	3.69
K^+	1.071 ± 0.069	1.006	0.273	3.69
K^-	0.984 ± 0.047	0.996	0.271	3.66
p	0.510 ± 0.018	0.545	0.150	3.63
\bar{p}	0.494 ± 0.017	0.536	0.148	3.62

Table 1: Experimental data on $dn/dy, |y| \leq 1$ by the CMS Collaboration [4] of charged pions, kaons, p , and \bar{p} production in central $p+Pb$ collisions at $\sqrt{s_{NN}} = 5$ TeV, together with the corresponding QGSM results. The parameter r is the ratio of the particle yields in $p+Pb$ and pp reactions. The predictions for pp collisions are also given.

Our predictions for hyperon and antihyperons production in pp and $p+Pb$ collisions at the same energy $\sqrt{s} = 5$ TeV are presented in Table 2.

The ratios of the inclusive densities of all secondary hyperons and antihyperons produced on Pb and hydrogen targets are practically the same as for secondary mesons production, with a $\sim 5\%$ accuracy (see tables 1 and 2). If our predictions will be experimentally confirmed, that would indicate that the main contribution to the processes of

hyperon and meson production has a similar nature.

particles	$p+\text{Pb } dn/dy_{y=0}$	$\text{pp } dn/dy_{y=0}$	r
Λ	0.307	0.0843	3.64
$\bar{\Lambda}$	0.303	0.0827	3.66
Ξ^-	0.0250	0.00676	3.70
Ξ^+	0.0248	0.00669	3.70
Ω^-	0.00143	0.000401	3.57
Ω^+	0.00142	0.000397	3.58

Table 2: The QGSM prediction for the densities of hyperons and antihyperons production $dn/dy_{y=0}$, in $p+\text{Pb}$ and pp collisions at $\sqrt{s} = 5.02$ TeV.

5 Conclusion

It is seen that the inelastic nuclear screening corrections at LHC energies are really large. All the ratios of inclusive densities of the secondaries produced in lead and hydrogen targets take values dn/dy , $|y| \leq 1 = 3.6\text{--}3.7$ (see Table 1), instead of the values dn/dy , $|y| \leq 1 = 7.5\text{--}8.0$ that one would expect in the absence of this effect (see Eq. 10).

In our approach it is naturally explained that the nuclear screening effects do not depend on the secondary produce particle, and they are practically the same (within our theoretical accuracy) for π^\pm , K^\pm , p , and \bar{p} production. This will be checked, and we are confident that confirmed, when the nuclear screening effects for the cases of hyperon production will be measured (see our predictions in Table 2).

Acknowledgements

We thank C. Pajares for his valuable comments.

This work has been supported by Russian RSCF grant No. 14-22-00281, by the State Committee of Science of the Republic of Armenia, Grant-15T-1C223, by Ministerio de Ciencia e Innovación of Spain under project FPA2014-58293-C2-1-P, and the Spanish Consolider-Ingenio 2010 Programme CPAN (CSD2007-00042), and by Xunta de Galicia, Spain (2011/PC043).

References

- [1] A. Capella, A. Kaidalov, and J. Tran Thanh Van, Heavy Ion Phys. **9**, 169 (1999).
- [2] C. Merino, C. Pajares, and Yu.M. Shabelski, Eur. Phys. J. **C59**, 691 (2009) and arXiv:0802.2195 [hep-ph].
- [3] B. Abelev *et al.*, ALICE Collaboration, Phys. Rev. Lett. **110** (2013) 3, 032301 and arXiv:1210.3615 [nucl-ex].

- [4] S. Chatrchyan *et al.*, CMS Collaboration, Eur. Phys. J. **C74**, 2847 (2014) and arXiv:1307.3445 [hep-ex].
- [5] C. Merino, C. Pajares and Y. M. Shabelski, Eur. Phys. J. C **73** (2013) 1, 2266 and [arXiv:1207.6900 [hep-ph]].
- [6] A.B. Kaidalov and K.A. Ter-Martirosyan, Sov. J. Nucl. Phys. **39**, 979 (1984) and Yad. Fiz. **39**, 1545 (1984); Sov. J. Nucl. Phys. **40**, 135 (1984) and Yad. Fiz. **40**, 211 (1984).
- [7] A.B. Kaidalov, Phys. Atom Nucl. **66**, 1994 (2003) and Yad. Fiz. **66**, 2014 (2003).
- [8] A.B. Kaidalov and O.I. Piskunova, Sov. J. Nucl. Phys. **41**, 816 (1985) and Yad. Fiz. **41**, 1278 (1985).
- [9] Yu.M. Shabelski, Sov. J. Nucl. Phys. **44**, 117 (1986) and Yad. Fiz. **44**, 186 (1986).
- [10] G.H. Arakelyan, A. Capella, A.B. Kaidalov, and Yu.M. Shabelski, Eur. Phys. J. **C26**, 81 (2002) and hep-ph/0103337.
- [11] C. Merino, M.M. Ryzhinskiy, and Yu.M. Shabelski, Eur. Phys. J. **B62**, 491 (2009).
- [12] G.H. Arakelyan, C. Merino, C. Pajares, and Yu.M. Shabelski, Eur. Phys. J. **C54**, 577 (2008) and arXiv:0709.3174[hep-ph].
- [13] A.B. Kaidalov and K.A. Ter-Martirosyan, and Yu.M. Shabelski, Sov. J. Nucl. Phys. **43**, 822 (1986) and Yad. Fiz. **43**, 1282 (1986).
- [14] Yu.M. Shabelski, Z. Phys. **C38**, 569 (1988).
- [15] V.A. Abramovsky, V.N. Gribov, and O.V. Kancheli, Sov. J. Nucl. Phys. **18**, 308 (1974) and Yad. Fiz. **18**, 595 (1973).
- [16] A.B. Kaidalov, Sov. J. Nucl. Phys. **45**, 902 (1987) and Yad. Fiz. **45**, 1452 (1987);
- [17] K.A. Ter-Martirosyan, Phys. Lett. **44B**, 377 (1973).
- [18] Yu.M. Shabelski, Sov. J. Nucl. Phys. **26**, 573 (1977) and Yad. Fiz. **26**, 1084 (1977); Nucl. Phys. **B132**, 491 (1978).
- [19] L. Bertocchi and D. Treleani, J. Phys. **G3**, 147 (1977).
- [20] J. Weis, Acta Phys. Polonica **B7**, 85 (1977).
- [21] T. Jaroszewicz et al., Z. Phys. **C1**, 181 (1979).
- [22] J.S. Trefil and F. von Hippel, Phys. Rev. **D7**, 2000 (1973).

- [23] Yu.M. Shabelski, Sov. J. Nucl. Phys. **45**, 143 (1987) and Yad. Fiz. **45**, 223 (1987); Z. Phys. **C38**, 569 (1988).
- [24] B.B. Black *et al.*, PHOBOS Collaboration, Phys. Rev. Lett. **85**, 3100 (2000).
- [25] K. Adcox *et al.*, PHENIX Collaboration, Phys. Rev. Lett. **86**, 500 (2001).
- [26] A. Capella, C. Merino and J. Tran Thanh Van, Phys. Lett. **B265** (1991) 415.
- [27] Yu.M. Shabelski, Z. Phys. **C57**, 409 (1993).
- [28] N. Armesto and C. Pajares, Int. J. Mod. Phys. **A15**, 2019 (2000).
- [29] A. Schwimmer, Nucl. Phys. **B94**, 445 (1975).
- [30] S. Ostapchenko, Phys. Rev. **D77**, 034009 (2008).
- [31] I. Bautista, C. Pajares, and J. Dias de Deus, Nucl. Phys. **A882**, 44 (2012).
- [32] I. Bautista, J. Dias de Deus, G. Milhano, and C. Pajares, Phys. Lett. **B715**, 230 (2012).
- [33] I. Bautista, C. Pajares, G. Milhano, and J. Dias de Deus, Phys. Rev. **C86**, 034909 (2012).
- [34] J. Dias de Deus, E. G. Ferreira, C. Pajares, and R. Ugoccioni, Eur. Phys. J. **C40**, 229 (2005).
- [35] C. Pajares, Eur. Phys. J. **C43**, 9 (2005).
- [36] L. Cunqueiro, J. Dias de Deus, E. G. Ferreira, and C. Pajares, Eur. Phys. J. **C53**, 585 (2008).
- [37] J. Dias de Deus and C. Pajares, Phys. Lett. **B695**, 211 (2012) and arXiv:1011.1099[hep-ph].
- [38] S. Chatrchyan *et al.*, CMS Collaboration, Eur. Phys. J. **C72**, 2164 (2012).
- [39] K. Aamodt *et al.*, ALICE Collaboration, Eur. Phys. J. **C71**, 1655 (2011).
- [40] B. Abelev *et al.*, ALICE Collaboration, Phys. Lett. **B 736**, 196 (2014).
- [41] J. Adam *et al.*, ALICE Collaboration, Eur. Phys. J. **C75**, 226 (2015).